Applied Catalysis B: Environmental 255 (2019) 117784

Contents lists available at ScienceDirect

Applied Catalysis B: Environmental

journal homepage: www.elsevier.com/locate/apcatb

Performance of boron-doped graphene aerogel modified gas diffusion electrode for in-situ metal-free electrochemical advanced oxidation of Bisphenol A

Panpan Wu[a,1], Yimei Zhang[a,b,1,*], Zhuang Chen[b], Yaxiao Duan[a], Yuxian Lai[a], Qinglu Fang[a], Fei Wang[b], Shuai Li[b]

[a] MOE Key Laboratory of Resources and Environmental System Optimization, College of Environmental Science and Engineering, North China Electric Power University, Beijing, 102206, China

[b] Laboratory of Environmental Remediation and Functional Material, Suzhou Research Academy of North China Electric Power University, Suzhou, Jiangsu, 215213, China

ARTICLE INFO

Keywords:
Boron-doped graphene aerogel
Metal-free catalysts
Gas diffusion electrode
Bisphenol A

ABSTRACT

Exploring the application of efficient metal-free catalysts in electrochemical advanced oxidation process (EAOPs) is of practical significance for environmental pollution treatment. Herein, the novel boron-doped graphene aerogel (BGA) modified gas diffusion electrode (GDEs) was prepared, characterized, and employed for bisphenol A (BPA) degradation in nonmetallic EAOPs. Boron doping could promote electrode property with a complete BPA removal within 60 min, which was attributed to the enhancement of H_2O_2 in-situ decomposition to •OH. An appropriate proportion of BGA (2.4%) represented more positive onset potential, favoring the remarkable improvement of oxygen reduction reaction (ORR) activity. The metal-free EAOPs on BGA-GDEs manifested smaller change in reaction rate ($0.0952\ min^{-1}$) compared with that of traditional Electro-Fenton (EF) process ($0.19115\ min^{-1}$) when the initial pH increased from 3.0 to 9.0, revealing that the catalytic activity of this metal-free system exhibited excellent stability over a wide pH range. In addition, the overwhelming superiority of stability was certified. Hence, the in-situ metal-free electrocatalysis on BGA-GDEs could be considered as an environment-friendly pollutant removal system without risk of metal contamination.

1. Introduction

Recently, generous researches have emerged and rapidly developed, which pave a new way for the design of innovative and comprehensive technology and its application in wastewater treatment [1–4]. Among these technologies, advanced oxidation process (AOPs) has been universally considered as an excellent method for the degradation of persistent organic pollutants due to its advantages of high efficiency, economy and environmental protection [5,6]. Particularly, Electro-Fenton (EF), which is one of the most representative AOPs, is on the basis of the constant in-situ production of H_2O_2 on the cathode (Eq. (1)), avoiding the collection, transportation and storage of H_2O_2, and then generates abundant •OH through adding the iron catalyst (Eq. (2)) [7].

$$O2 + 2H^+ + 2e^- \rightarrow H2O2 \quad (1)$$

$$Fe^{2+} + H2O2 \rightarrow Fe^{3+} + OH^- + \bullet OH \quad (2)$$

In the past few years, the rapid progress of EF technology has benefited from the successful development and application of high-efficiency catalysts. Thereinto, research on metal-based catalysts is especially fruitful. A series of catalysts containing iron species or transition metal oxides have been successfully applied to the EF system for organic pollutants degradation [8–11]. Despite continuous improvement in catalytic performance, these metal-based catalytic systems have two inherent defects seemed inevitable. First, the pH adaptation range of EF is narrowly limited to 2.5 ~ 3.5 to avoid the catalyst coagulation at high pH and the appearance of adverse reactions in strong acid condition [12–15]. Second, the secondary pollution caused by metal leaching is always unavoidable. The increase of treatment cost and follow-up environmental problems resulted from these two inherent defects seriously restrict the application of metal EF catalysis [16–18]. Therefore, it is highly desirable to develop the metal-free

* Corresponding author at: Suzhou Research Academy of North China Electric Power University, Suzhou, Jiangsu, 215026, China.
E-mail address: angym@ncepu.edu.cn (Y. Zhang).

[1] These authors contributed equally to the work.

https://doi.org/10.1016/j.apcatb.2019.117784
Received 17 April 2019; Received in revised form 24 May 2019; Accepted 27 May 2019
Available online 29 May 2019

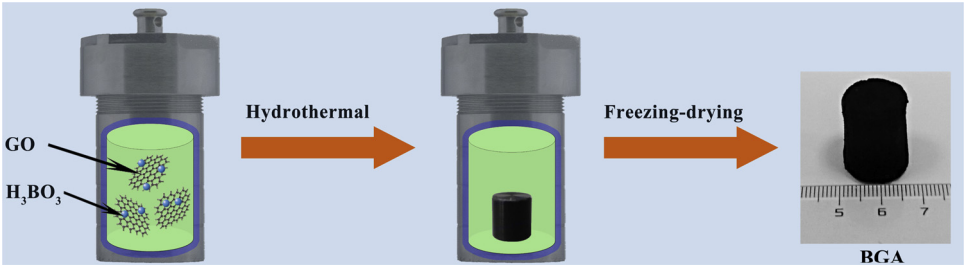

Fig. 1. The process of the as-prepared BGA catalyst.

catalysts in terms of the practicability and eco-friendliness for wastewater treatment.

Among the metal-free catalysts, carbon materials deserve to be preferred because of their diverse structure, accessibility and innocuousness to ecosystems. The π-conjugated sp^2 hybridize carbon and surface functional groups of carbon materials have been identified as active sites for H_2O_2 decomposition, which play the role of electron transfer mediators, similar to the electron transfer mechanism of metal catalysts in traditional EF reactions [19–21]. In this regard, graphene aerogel (GA) is rich in the π-conjugated sp^2 hybridize carbon, which is an appealing candidate for electrochemical advanced oxidation processes (EAOPs). Furthermore, GA has characteristics of both the interconnected three-dimensional (3D) porous structure of aerogel and high conductivity of graphene [22–24]. Owing to the unique structure, GA provided two major advantages for oxygen reduction reaction (ORR) and H_2O_2 decomposition into •OH: (i) GA has a porous network which is more suitable to anchor O_2, thereby improving the ORR for H_2O_2 production; (ii) the large surface area of GA offers more active sites for the H_2O_2 decomposition reaction. In addition, GA also exhibits wonderful modification. Remarkably, doping non-metallic heteroatoms (such as N, B, P, S, and I) into carbon materials, enormously enhancing their electrocatalysis properties due to their electrical neutral fracture and charge modulation, has increasingly become a research hotspot. [25–30]. Among the potential dopants, doping boron atoms in graphene presents impressive electrochemical performance for ORR [31], and the incorporation of B atom into carbon skeleton can alter original sp^2-hybridized structure and form new active regions in favor of activating reactions [32,33]. As a result, B-doping is considered to overwhelmingly improve the electrochemical property and catalytic capacity of GA for EAOPs. According to our knowledge, the boron-doped graphene aerogel (BGA) is reported for the first time as the metal-free catalyst for in-situ metal-free EAOPs. This study finding would provide new insights into the non-metallic catalysis and be expected to open a new avenue to strategically design highly active and performance-oriented metal-free electrocatalytic materials for EAOPs.

Herein, the modified gas diffusion electrode with boron-doped graphene (BGA-GDEs) was prepared by the simple hydrothermal process for BPA removal from wastewater. The obtained BGA was characterized by Scanning electron microscopy (SEM), X-ray diffraction (XRD), Raman spectra, SEM energy-dispersive X-ray spectroscopy (EDS), X-ray photoelectron spectroscopy (XPS), and the electrocatalytic behavior of the electrode for ORR was assessed by linear sweep voltammetry (LSV). Three parameters, such as BPA removal efficiency, H_2O_2 production, and •OH amount, were detected to analyze the electrocatalytic performance of as-prepared electrodes of ORR. The catalytic activities of catalyst-free electrode, GA-GDEs and BGA-GDEs were then investigated. Subsequently, the effects of BGA doping mass and pH value on electrocatalytic performance were assessed. Moreover, metal-free catalysis was compared with traditional EF process, and the stability performance of BGA-GDEs was further evaluated. Finally, the intermediates of BPA generated during the metal-free EAOPs were identified, and the possible reaction mechanism was also put forward.

2. Experimental

2.1. Material

Graphene oxide (GO), Bisphenol A (BPA), methanol (HPLC, ≥99%), sulphuric acid (H_2SO_4, ≥99%), NaOH, and Na_2SO_4 were obtained from Sinopharm Chemical Reagent Co., China. Boric acid (H_3BO_3) and other chemicals were purchased from Shanghai Chemical Reagent Factory. Deionized water was used during the whole experiments. All the chemicals employed in the experiments were analytical grade and not further purified.

2.2. Fabrication of BGA

GO was prepared from powder-like graphite via the Hummers method [34]. Boric acid was selected as the boron resource. As shown in Fig. 1, BGA was synthesized by a simple hydrothermal process. To be specific, graphene oxide was scattered in deionized water to reach the concentration of 2.0 mg mL^{-1}. The 300 mg of H_3BO_3 were mixed with 30 mL of the above homogeneous solution and sonicated for 15 min until dissolution. Subsequently, the well-distributed dispersion was shifted into a Teflon-lined autoclave and conducted hydrothermal treatment at 180℃ for 12 h to acquire boron-doped graphene hydrogels. After cooling to room temperature, the composites were repeatedly washed with deionized water and ethanol, respectively. Finally, the samples were acquired through freeze-drying for 48 h. Analogously, graphene aerogels (GA) also were synthesized without adding boric acid.

2.3. Characterization

SEM (S-4700, Hitachi Limite) was performed to analyze the morphology of the samples. The crystal structure was characterized by XRD using D/MAX-2400 X-ray diffractometer from Janpan consisted of Ni-filtered Cu Kα radiation. The nitrogen adsorption-desorption was carried out to measure the specific surface area adopting the BET method (Novae series, Quantachrome Co., USA). Raman spectra was detected using a spectrometer (Renish Modular Raman spectrometer, France). XPS was performed to determine the crystalline structure of BGA using Mono Al Ka radiation. EDS mapping was conducted on a Focused Ion Beam Scanning Electron Microscope (JIB 4500 MultiBeam).

2.4. Preparation of gas diffusion electrode

The stainless steel meshes (SSM, 3.0 cm × 2.0 cm) was adopted as the substrate and current collector to prepare the gas diffusion electrode. GA and BGA were used to form the catalyst layer of electrodes, which were denoted as GA-GDEs and BGA-GDEs, respectively. Concretely, the fabrication process of BGA-GDEs was depicted as follows. Initially, 2.0 mg BGA was mixed with 80 mg acetylene **black** (CB) and PTFE emulsion (CB:PTFE = 6:1) in ethanol by ultrasonication for 20 min to form a well-dispersed ink. Afterwards, the above ink was concentrated by evaporating ethanol at 75℃ to obtain the wet slurry,

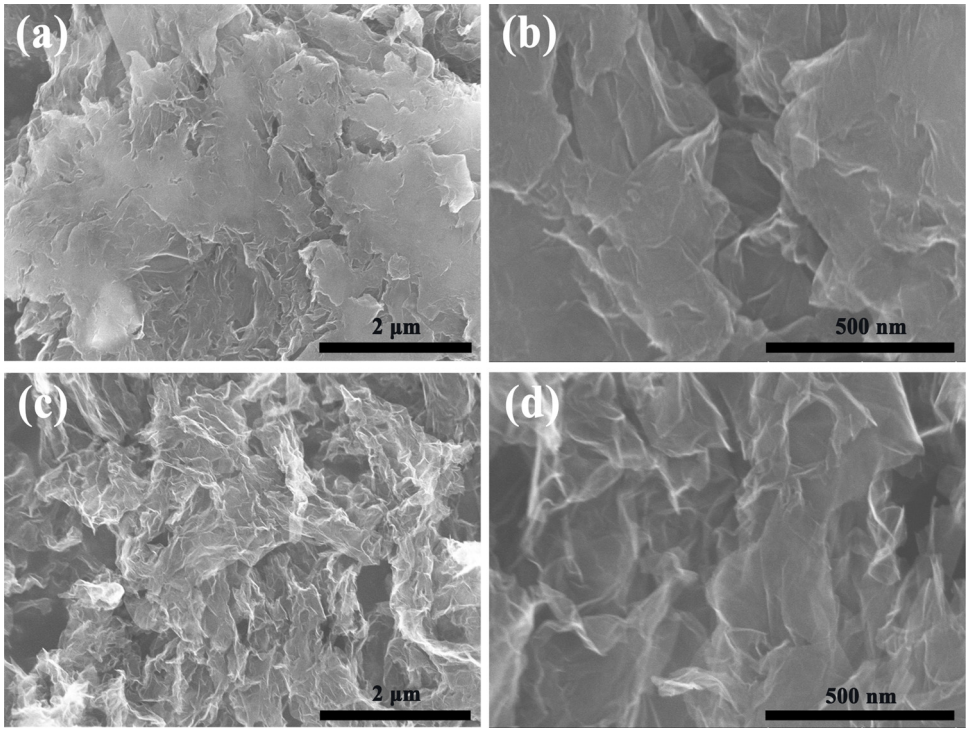

Fig. 2. SEM images of GA (a and b), BGA (c and d).

which was then coated onto the two sides of SSM. Eventually, the as-prepared BGA-GDEs was obtained after annealed at 330℃ for 10 min. During the heat treatment process, the good mixture of thermally melt PTFE with carbon **black** and BGA enabled the electrode to achieve a remarkable hydrophobic effect. For comparison, the electrode only with carbon **black** and PTFE without catalyst was also prepared via the same procedure.

2.5. Electrochemical measurements

Electrochemical workstation (Shanghai CHI 660E) with a three-electrode system was employed to measure the electrochemical properties of BGA-GDEs. The as-prepared electrode (3.0 cm × 2.0 cm) was adopted as working electrode, platinum electrode (2.5 cm × 2.5 cm) as counter electrode, and a saturated calomel electrode (SCE) as reference electrode, respectively. The LSV measurement was conducted in the 0.05 M Na_2SO_4 solution with a scanning rate of 10 mV/s under a potential range from 0 to −1.4 V.

2.6. Electrochemical ORR and BPA degradation

Electrochemical degradation toward BPA was carried out in a three-electrode electrolysis reactor (6.5 cm × 5.0 cm × 5.0 cm) using chronopotentiometry of the electrochemical workstation. The as-prepared electrode (3.0 cm × 2.0 cm) was adopted as working electrode, platinum electrode (2.5 cm × 2.5 cm) as counter electrode, and a SCE as reference electrode, respectively. Typically, BPA was used as the target pollutant with an initial concentration of 10 mg L^{-1} and volume of 50 mL. The initial pH value was adjusted as 3.0, and 0.05 M Na_2SO_4 was applied as supporting electrolyte. Before the degradation experiment, air was provided at a flow rate of 0.3 L min^{-1} for 10 min in the above-mentioned BPA solution. The experiments were carried out under 4.5 mA cm^{-2} constant current density with continuous aeration. Within a specified time interval, 1.0 mL of samples were taken out and filtered through 0.22 μm membrane filter for analysis.

2.7. Analysis method

The BPA amount was detected through LC210A High Performance Liquid Chromatography (HPLC) from Shanghai. The instrument was equipped with a Welchrom C18 reversed-phase column (4.6 mm × 250 mm, 5 μm) and a diode array UV–vis detector. The mobile phase was methanol/water (70:30, v/v), and the constant flow rate was 1.0 mL min^{-1}. The detection wavelength was selected as 280 nm. The sample injection volume was chose as 20 μL. On the basis of the potassium titanium oxalate method, a UV–vis spectrophotometer (752 N) was adopted to quantify the concentration of H_2O_2 at a wavelength of 400 nm [35].

For further quantitative calculation of free radicals, •OH were trapped with dimethyl sulfoxide (DMSO) [36]. Firstly, the formaldehyde was generated quantitatively by the reaction between •OH and DMSO, and then reacted with 2,4-dinitrophenylhydrazine (DNPH) at pH 4.0 to form the corresponding hydrazone (HCHO-DNPH), which was analyzed by HPLC. The mobile phase was methanol/water (60:40, v/v), and the constant flow rate was 1.0 mL min^{-1}. The detection wavelength was selected as 355 nm. The sample injection volume was chose as 10 μL. Total organic carbon (TOC) was measured using a DR900 analyzer (Hach company, USA).

3. Results and discussion

3.1. Characterization of modified electrode

The morphologies of GA and BGA composites were explored through SEM. It could be distinguished that the GA sample surface was relatively smooth with several wrinkles layers while BGA exhibited the 3D interconnected framework with porous structure (Fig. 2a and c). The further magnified image in Fig. 2b and d demonstrated that more crumpled layers appeared in BGA materials compared with GA composites. It was ascribed to the fact that the incorporation of boron atoms into the graphene nanosheets could yield considerably denser interconnected channels. This unique structure showed potential to form more electronic bridges between boron atoms and adjacent graphene

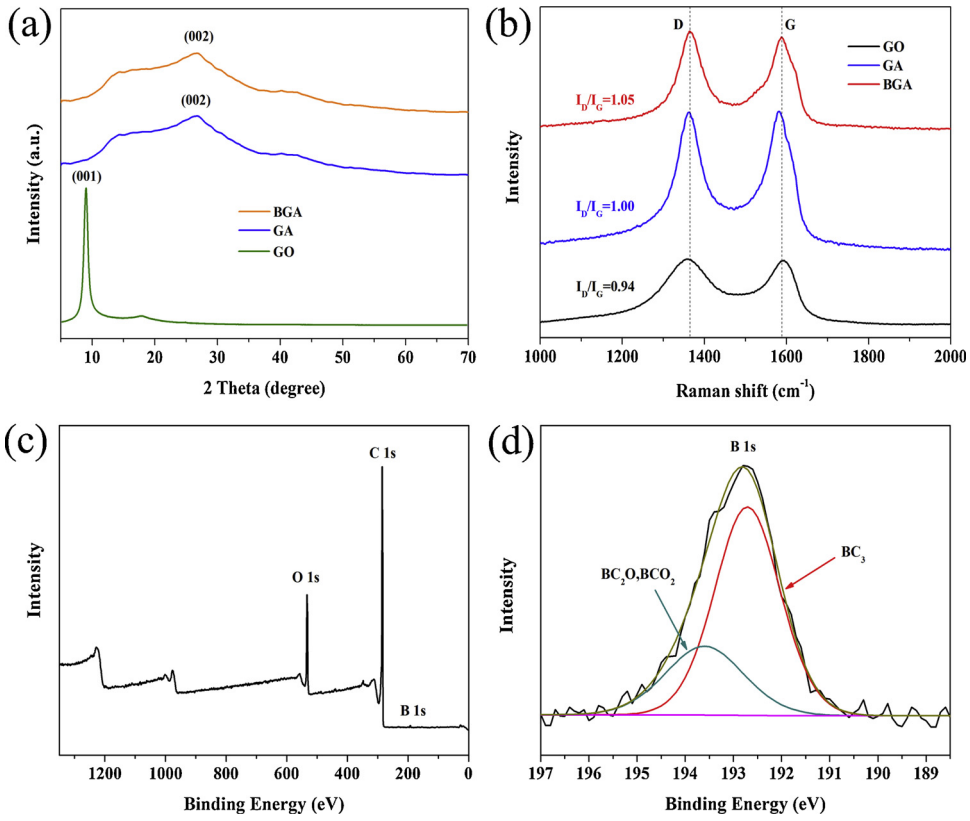

Fig. 3. XRD patterns of GO, GA and BGA (a); Raman spectra of GO, GA, BGA (b); XPS survey spectra of BGA (c); B 1 s peak of XPS spectrum of BGA (d).

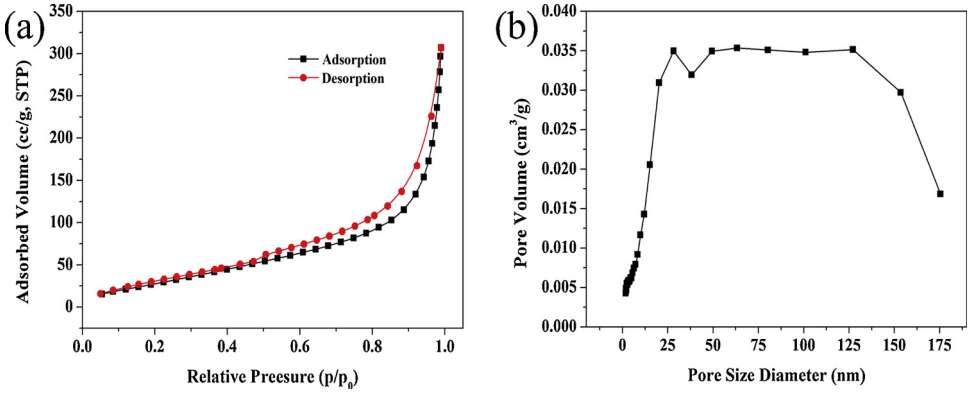

Fig. 4. N_2 adsorption/desorption isotherms (a); The pore size distribution plot of BGA (b).

aggregates, which could accelerate electron transfer and thus improve electrocatalytic performance.

The XRD patterns of GO, GA, and BGA samples were depicted in Fig. 3a. The characteristic peak appeared at 9.2° and the interlayer distance was 0.96 nm, which stemmed from GO (001). After hydrothermal treatment, this peak completely disappeared and a new peak at 26.2° with an interlayer distance of 0.34 nm was found labeled as (002) plane of graphite [37], which was attributed to the deoxidization of GO during hydrothermal process. Additionally, boron atoms incorporation allowed the peak to shift higher. The XRD spectra of BGA showed characteristic diffraction peak at 26.7°, corresponding to an interlayer distance of 0.33 nm, indicating that boron-doping process partially restored the graphitic crystal structure.

The Raman spectra presented the disorder degree of the three as-prepared materials. As shown in Fig. 3b, the samples all possessed the typical bands at approximately 1360 cm^{-1} and 1590 cm^{-1}, which referred to the well-defined D-band and G-band, respectively [38]. The D/G peak intensity ratio (I_D/I_G) obtained from GO, GA, and BGA were 0.94, 1.00, and 1.05, respectively. Furthermore, BGA exhibited the slightly broader D band and up-shifted G band position than GA. These observations illustrated that the introduction of boron atoms could lead to more structural defects and disorders within graphene.

The XPS characterization was carried out to explore the chemical composition and boron content of BGA. As displayed in Fig. 3c, three principal peaks were monitored at the binding energy of 193, 285 and 533 eV, corresponding to the characteristic B1s, C1s, and O1s, respectively. The amount of boron atom accounted for approximately 1.66% in BGA composite, demonstrating that boron atoms were successfully introduced into the hexagonal carbon network during the hydrothermal process. Moreover, Fig. 3d presented the existence of three distinct forms of B atoms in the target composite. The intense peak at 192.7 eV was assigned to $-BC_3$ bond, which was formed by the substitution of B for C in the hexagonal lattice [39]. The weak signal at higher binding energy position of 193.6 eV was ascribed to the presence of borinic ester

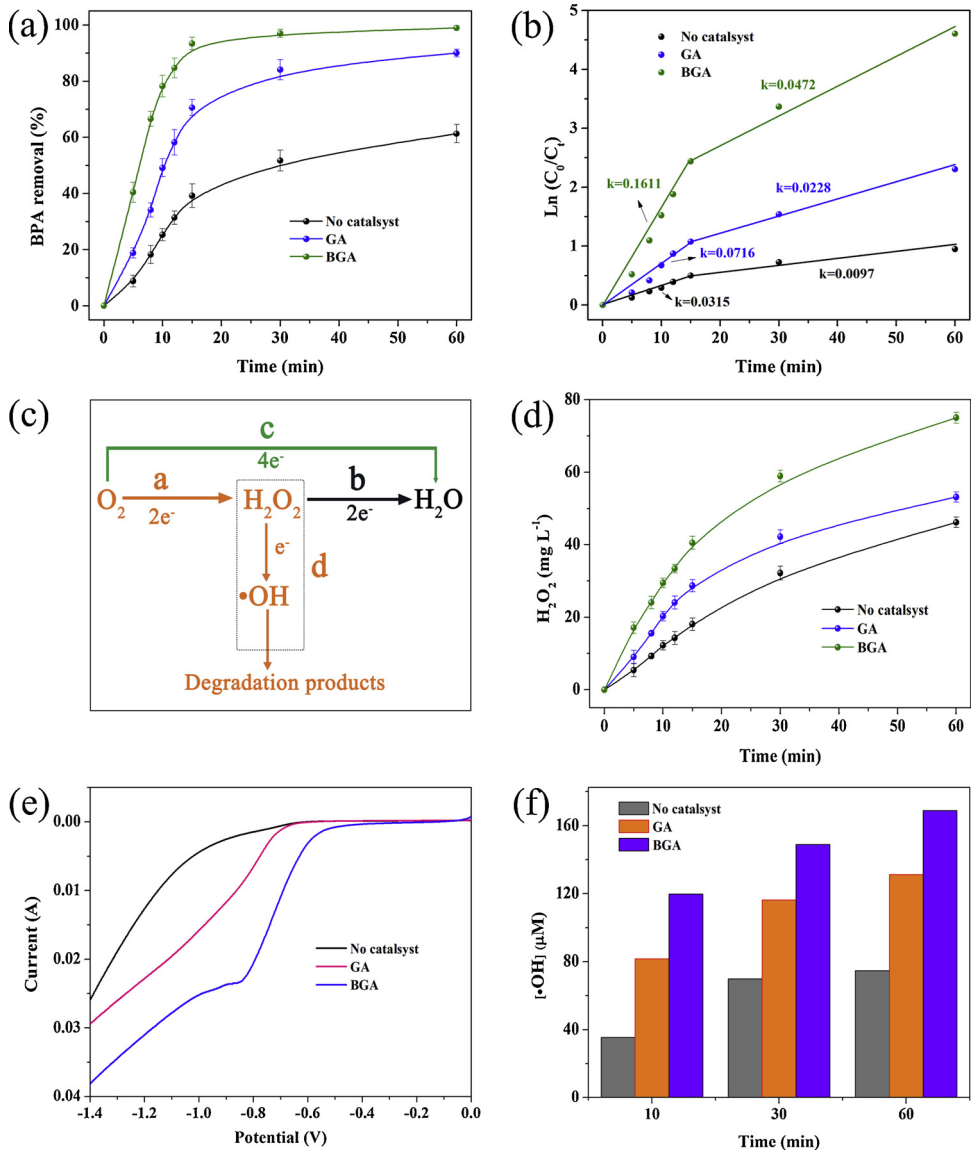

Fig. 5. The degradation of BPA in the EAOPs on catalyst-free electrode, GA-GDEs and BGA-GDEs, respectively (a); Pseudo-first-order degradation of BPA versus time under various conditions in batch processes (b); Schematic illustration of possible mechanisms of EAOPs (c). The performance of H_2O_2 generation with no catalyst, GA and BGA as the catalyst, respectively (d); LSV curves (e). The concentration of ▪OH on the three electrodes in EAOPs (f).
Conditions: initial BPA concentration: 10 mg L^{-1}; V = 50 mL; pH = 3; Na_2SO_4: 50 mM; Current density: 45 A m^{-2}.

(–BCO_2) and boronic acid (–BC_2O) moieties [40].

The N_2 adsorption-desorption isotherm and pore diameter distribution of BGA were further measured. As shown in Fig. 4a, the N_2 sorption curve of the as-prepared composite presented a typical type IV isotherm and wide hysteresis area, illustrating that BGA exhibited macroporous and mesoporous structure [41]. It was consistent with the observation of Barret-Joyner-Halenda pore diameter distribution (Fig. 4b), suggesting the wide pores distribution in the composites. The specific surface area of BGA was measured as 123.18 $m^2 g^{-1}$, and the pore volume was calculated as 0.299 $cm^3 g^{-1}$. These results justified that BGA composite possessed porous framework, which was expected to serve as active sites to accelerate the free radicals generation, thereby promoting the contaminants degradation efficiency.

3.2. Electrocatalytic Properties on different metal-free electrode in EAOPs

The electrocatalytic activities on catalyst-free electrode, GA-GDEs and BGA-GDEs in EAOPs were investigated employing the extensively studied BPA [42,43] as the target pollutant. As revealed in Fig. 5a, BPA was almost completely degraded within 60 min on BGA-GDEs, while the removal efficiency with GA-GDEs and catalyst-free electrode were 88.92% and 61.35%, respectively. It could be discovered from Fig. 5b that the metal-free catalytic degradation of BPA consisted of a two-step process and each stage followed a pseudo-first-order kinetics, exhibiting the relatively rapid catalytic reaction in the first 15 min. The sum of two-stage reaction rate constant (k) at BGA-GDEs was calculated to be 0.2083 min^{-1}, which was two-fold of GA-GDEs (0.0944 min^{-1}) and four times that of catalyst-free electrode (0.0412 min^{-1}). These results demonstrated that BGA-GDEs possessed more excellent degradation performance for BPA compared with GA-GDEs and catalyst-free electrode.

The possible EAOPs mechanism in the metal-free catalytic process was displayed in Fig. 5c. The additional O_2, as the initial source of reaction, could be transformed through two pathways. The O_2 produced H_2O_2 by $2e^-$ ORR (a) and the parallel-sequence reactions proceeded with the following processes: including reduction of H_2O_2 to H_2O (b), further decomposition of H_2O_2 to •OH (d). Another way was to directly convert O_2 to H_2O (c) by $4e^-$ ORR. These three different routes (b, c, d)

competed with each other. The extraordinary degradation capability of BGA-GDEs was mainly ascribed to the high yield of •OH generated by the in-situ activation of H_2O_2 produced at the electrode (route d).

Accordingly, the H_2O_2 amount on the BGA-GDEs presented the outstanding ability of 75.03 mg L^{-1} after 60 min, while the H_2O_2 production with GA-GDEs and catalyst-free electrode reached 58.42 mg L^{-1} and 46.53 mg L^{-1}, respectively (Fig. 5d). The results indicated that the boron-doping in graphene contributed to promoting the ORR activity toward H_2O_2 formation (Eq. (3)), which was consistent with the LSV measurement. As clearly depicted in Fig. 5e, the ORR onset potentials of catalyst-free electrode, GA-GDEs, and BGA-GDEs were labeled as −0.90 V, −0.75 V, and −0.50 V, respectively. The as-prepared BGA-GDEs possessed considerably more positive onset potential than the other electrodes, reflecting a significant improvement of electrochemical activity and a more facile electrocatalytic process for ORR [44,45]. This phenomena verified that BGA-GDEs exhibited distinct superiority with regard to H_2O_2 generation. Previous studies had shown that separate H_2O_2 hardly decomposed BPA [46–48], so high-capacity of H_2O_2 production was not the immediate cause of superior electrode activity.

The •OH accumulation was further determined to investigate its contribution in metal-free EAOPs. It could be observed in Fig. 5f that the •OH amount attained 121.73 μM at 10 min on BGA-GDEs, which was one and a half times of GA-GDEs (80.57 μM) and approximately four-fold greater than that on catalyst-free electrode (32.38 μM). The •OH concentration increased as the reaction proceeded and reached 169.89 μM at 60 min on BGA-GDEs, and the distinction of the •OH amount generated on the three electrodes was in agreement with the BPA degradation efficiency. The H_2O_2 yield they generated was sufficient for the assignment of •OH (Eq. (4)). Therefore, we deduced that the ability of three kinds of electrodes to catalyze H_2O_2 decomposition towards •OH was the major contributor to the differentiated behaviors. The remarkable activation of H_2O_2 toward •OH on BGA-GDEs might be due to the boron incorporation in graphene nanosheets. This well corresponded to the discovery from Fig. S1 that boron atoms were uniformly doped in graphene. B-doping could destroy sp^2 hybridized structure of carbon and created active sites, thereby the new BGA active region accelerated the activation rate of free radicals. It should also be noted that based on the analysis of the onset potential aforementioned, the boron doping in graphene could change the electron distribution and enhance the charge density at some point on the surface, which stimulated the activation of H_2O_2 to •OH.

$$O2 + 2H^+ + 2e^- \rightarrow H2O2 \quad (3)$$

$$H_2O_2 + e^- \rightarrow OH^- + \bullet OH \quad (4)$$

According to the above discussion, the primary mechanism of electrocatalysis removal BPA with BGA-GDEs was proposed. As shown in Fig. 6, there was one principal pathway for electrochemical reactions between migrated O_2 and electrons on the electrode. The two-electron

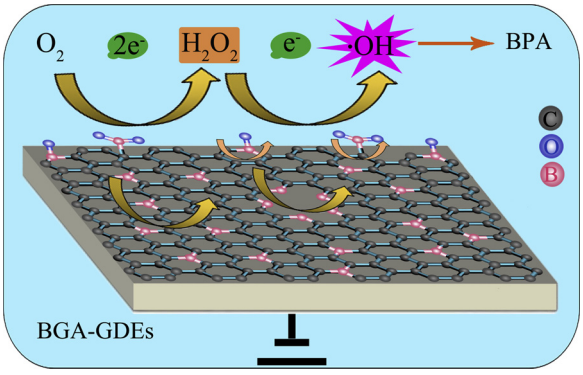

Fig. 6. Schematic illustration of the in-situ metal-free EAOPs with BGA-GDEs.

reduction reaction of O_2 was conducted to produce H_2O_2, and then the electrons were transformed to H_2O_2 in-situ activation forming •OH. Notably, the diverse "activation regions" were introduced as result of the formation environments of various B-doped states in graphene nanosheets. Three distinct forms of -BC_2O, -BCO_2, and -BC_3 bond existed in BGA-GDEs, and its excellent electrocatalytic performance might be attributed to the synergistic effect of these B-bond configurations. Among them, B atom with positive charge polarization substitution position (-BC_3) was the dominant species occupying 71.64%, and it could be served as the activation region of electron transfer to migrate electrons rapidly and effectively [49]. In contrast, the more electrophilic B derivatives (–BC_2O, –BCO_2), which mainly located at the edge or defect sites, could act as the preferred sites for O_2 absorption. These two bonds could promote O_2 adsorption kinetics and extract electrons to activate O—O bond decomposition, thus enhancing the production of active intermediates [50]. This was consistent with Di Valentin's recent theoretical research results [51,52].

3.3. Effect of different mass of BGA doping on BPA degradation

The effect of the BGA doping contents on BPA degradation was evaluated in the metal-free EAOPs process. As presented in Fig. 7a, BPA was almost completely removed within 60 min when the BGA doping ratio was 2.4%, whereas the BPA degradation efficiency depressed to 91.71% and 61.33% with the catalyst amount lessening to 1.2% and 0. Further BGA content increase from 1.2% to 5.9%, 11.1%, and 15.8% resulted in the decline to 89.20%, 81.74%, and 73.82%, respectively. The similar activity orders of both H_2O_2 and •OH production were observed from Fig. 7b and c. These observations demonstrated that an appropriate proportion of BGA could effectively promote the electrocatalytic activity, while the insufficient or excessive caused its depression. Hence, 2.4% of BGA mass was beneficial to obtain an optimal degradation efficiency.

These results might be explicated in the following two aspects. One the one hand, the presence of active sites exerted vital influence on the free radicals generation. The geometric area of the electrode is definite. A small amount of BGA corresponded to relatively few effective sites, which were not enough to trigger the reaction. Excessive BGA dosage enabled the accessible active sites to be occupied, so that the added O_2 as the initial source of reaction was not sufficiently filled in the BGA-GDEs, thereby inhibiting the subsequent reaction process. Besides, excess amount of BGA may accelerate the reaction process of route b and c (Fig. 5c) [53], which will affect the effective generation of •OH. On the other hand, the ORR activity was significantly affecting the electrode performance. As displayed in Fig. 7d, all boron-doped electrodes presented higher response currents than unmodified electrode. Among these boron-doped electrodes, the as-fabricated 2.4% BGA-GDEs performed a stronger current response and more positive onset potentials than other electrodes. These observations indicated that an appropriate proportion of BGA was conducive to the remarkable improvement of ORR activity, which determined the electron migration capability.

3.4. The performance comparison between metal-free EAOPs and traditional EF

The behavior of metal-free system at BGA-GDEs was compared with traditional EF process at the catalyst-free electrode toward BPA decomposition under different pH conditions. As presented in Fig. 8a, BPA degradation efficiencies on BGA-GDEs achieved 99.56%, 96.12%, 95.50%, and 94.88% at pH 3.0, 5.0, 7.0, and 9.0, respectively. The removal rate only decreased by 4.68% as the pH increased from 3.0 to 9.0, illustrating that the variety of pH had no significant effect on the BPA removal in metal-free catalysis. However, quite different phenomena have been noticed in the EF process, as shown in Fig. 8c. The BPA removal rate reached 91.65% at pH 3.0 with the amount of Fe^{2+} of 2.0 mg L^{-1} as the maximum leaching amount allowed by European

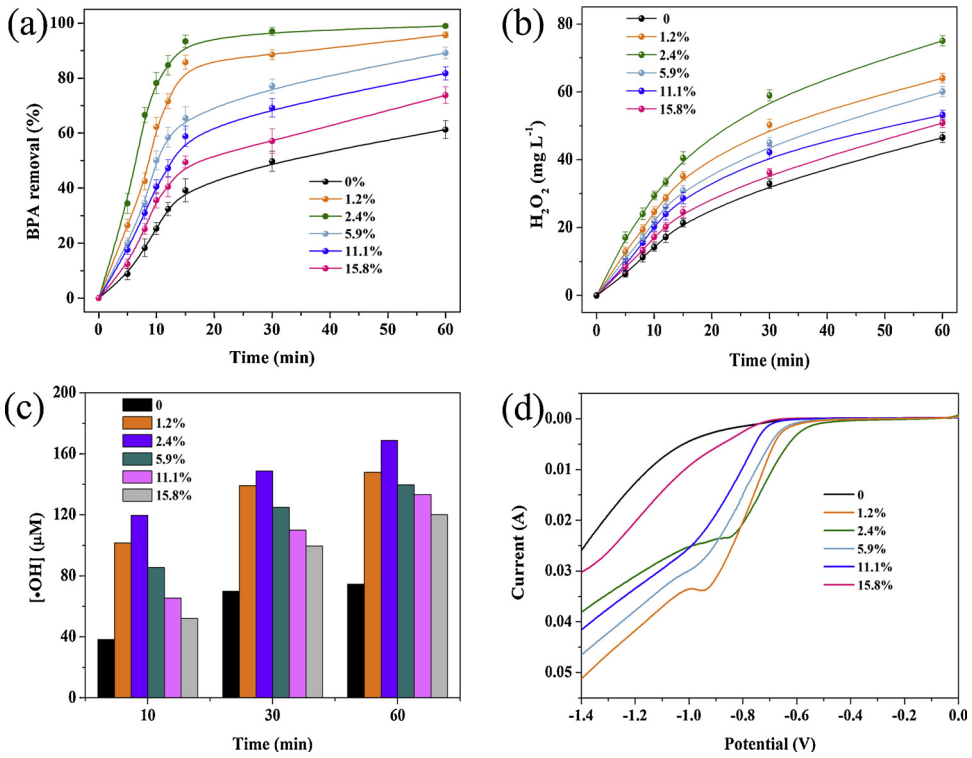

Fig. 7. The effect of doping amount of the BGA catalyst on BPA degradation in the EAOPs (a); The performance of H_2O_2 generation with different doping amount of the BGA catalyst (b); The concentration of ▪OH on different electrodes in EAOPs (c). LSV curves of different electrodes (d).

Union [54], which was not as excellent as that of metal-free EAOPs. When the Fe^{2+} addition was increased to 5.0 mg L^{-1}, BPA was removed with efficiency up to 98.45%, and its degradation trend was similar to that of the metal-free catalysis at pH 3.0. In fact, although increasing iron content can improve BPA removal efficiency, it will inevitably be accompanied by more iron leaching and then cause severe second contamination. Here, for comparison, 5.0 mg L^{-1} of Fe^{2+} was used to study the pH effect in EF system. The study found that the

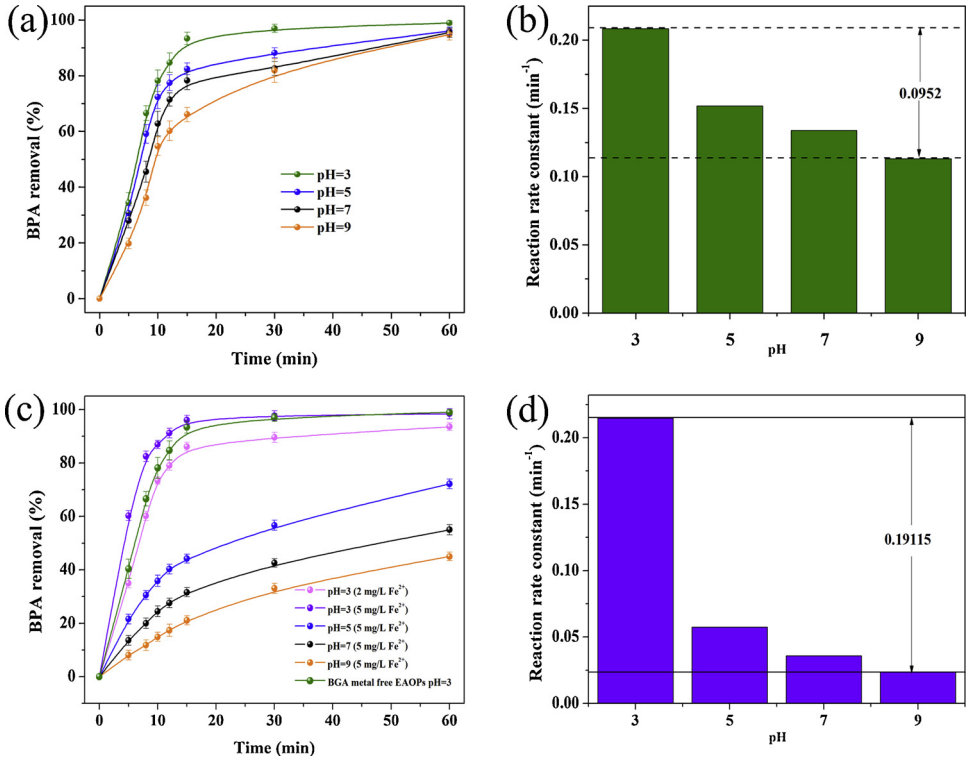

Fig. 8. The effect of pH on BPA degradation in the in-situ metal-free EAOPs (a); Reaction rate constant of BPA degradation in the in-situ metal-free EAOPs (b); The BPA degradation efficiency in traditional EF process under different conditions (c); Reaction rate constant of BPA degradation in traditional EF process (d).

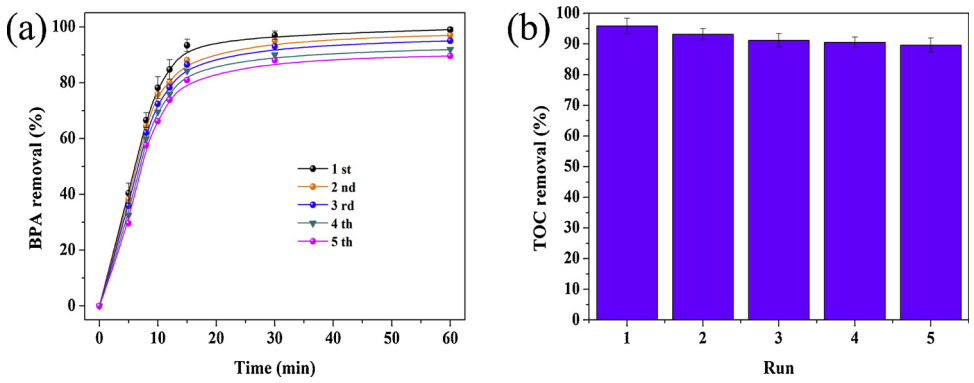

Fig. 9. The stability of BGA-GDEs for BPA degradation (a). The TOC removal rate through repeated experiments (b).

removal rate dramatically decreased to 72.24%, 55.32%, and 44.13% with the initial pH increased to 5.0, 7.0, and 9.0. The removal efficiency in EF process decreased by 54.32%, far exceeding the metal-free system (only 4.68%), indicating that a critical limitation of EF was the narrow pH adaptation range of around 3.0. To gain more insight, the kinetics rate (k) was investigated with the change of pH. As shown in Fig. 8b and d, the change of k value in EF process (0.19115 min^{-1}) was also more twice than that of metal-free EAOPs (0.0952 min^{-1}), showing that the catalytic activity of this metal-free system exhibited excellent stability over a wide pH range. In conclusion, the in-situ metal-free catalysis system on BGA-GDEs conquered the two inevitable disadvantages of traditional EF on the premise of maintaining high catalytic efficiency, which not only enlarged the working pH range, but also avoided the secondary pollution.

3.5. Stability performance of BGA-GDEs

The reusability of BGA-GDEs was investigated in five consecutive runs for BPA treatment, in which ethanol was applied to regenerate electrode after each operation. As could be seen from Fig. 9a, the first used electrode almost completely degrade BPA within 60 min, and it slightly reduced to 97.13%, 94.82%, 91.90%, and 89.65% after the second, third, fourth, and fifth reuse. The outstanding superiority of the stability certified that the metal-free electrocatalysis at BGA-GDEs would be regarded as an environment-friendly pollutant removal system without adding metal-based catalysts and producing metallic pollution.

The TOC removal was further assessed through batch experiments. As displayed in Fig. 9b, it could be observed that the trend resembled that of BPA removal. The TOC elimination value was 95.91% in the first run and attained 89.58% after the fifth reuse, revealing that the TOC removal efficiency on the as-prepared electrode maintained stability. The advantages possessed by BGA-GDEs could provide insights into the design of novel metal-free electrodes with enhancing catalytic activity in refractory organic wastewater treatment.

3.6. Possible degradation mechanism toward BPA during the metal-free EAOPs on BGA-GDEs

The intermediate products of BPA generated during the metal-free EAOPs were identified via HPLC. As displayed in Fig. 10, only BPA was found at the retention time of 6.18 min in the initial BPA solution. After the degradation reaction began, four cardinal products were detected, corresponding to p-benzoquinone (3.40 min), phenol (3.85 min), 4-isopropylphenol (4.30 min), and 4-hydroxyacetone (4.65 min), respectively [55,56]. The BPA characteristic peak area constantly decreased and nearly eliminated completely after 60 min, and the content of the above-mentioned four intermediates increased first and then decreased. Based on this, the degradation mechanism could be interpreted as

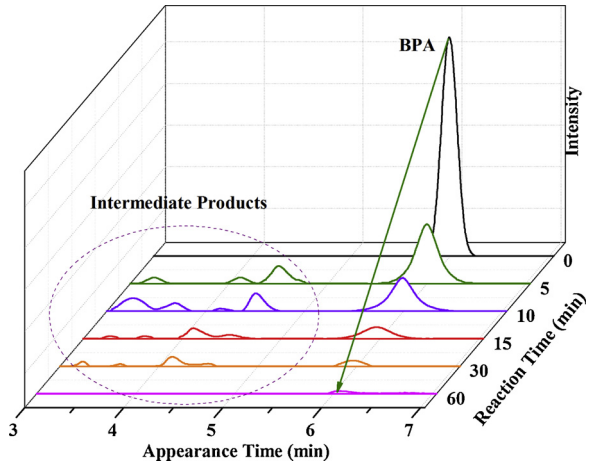

Fig. 10. HPLC spectrogram of BPA during the degradation of BPA with BGA-GDEs.

follows. First of all, BPA was attacked by •OH, losing an electron to form bisphenol A radicals [57]. Secondly, BPA radicals were resolved into 4-isopropylphenol and phenol through the C—C bond fracture between isopropyl and benzene ring of bisphenol A radical [58,59]. Afterwards, 4-isopropylphenol and phenol were transformed into 4-hydroxyacetophenone and p-hydroquinone, which was easily converted to p-phenylquinone. Furthermore, aromatic intermediates were vulnerable, it inevitably produced downstream short-chain acids under the constant attack of the free radicals. These short-chain acids can not be detected as a result of the retention time limitation of HPLC. Eventually, the short-chain acids could be further mineralized into CO_2 and H_2O.

4. Conclusions

In the present work, BGA-GDEs was successfully prepared and possessed fantastic electrocatalytic performance compared with the catalyst-free electrode and GA-GDEs. The doped amount of 2.4% BGA was beneficial to obtain an outstanding degradation efficiency of almost complete BPA degradation within 60 min. The research indicated that an appropriate proportion of BGA doping in graphene could be conducive to promoting the ORR activity toward H_2O_2 formation and catalyzing H_2O_2 decomposition towards •OH. Moreover, the in-situ metal-free catalysis system on BGA-GDEs conquered the disadvantages of traditional EF, which not only enlarged the working pH range, but also avoided the secondary pollution. After five cycles, the BPA removal rate remained about 89.65% and TOC elimination value attained 89.58%, demonstrating that the modified electrode exhibited outstanding stability. Finally, the degradation intermediates of BPA were determined, and the possible reaction mechanism was also put forward.

Overall, BGA-GDEs can potentially guide the development direction of metal-free EAOPs for wastewater treatment.

Acknowledgment

The authors would like to express their appreciation for research funding provided by the National Natural Science Foundation of China (Grant No. 51878272) and the National Key R&D Program of China (No. 2017YFB0603400).

Appendix A. Supplementary data

Supplementary material related to this article can be found, in the online version, at doi:https://doi.org/10.1016/j.apcatb.2019.117784.

References

[1] Y.M. Shao, L.C. Zhou, Q. Wu, J. Hazard. Mater. 339 (2017) 418–426.
[2] P.R. Gogate, A.B. Pandit 8 (2004) 501–551.
[3] R. Andreozzi, V. Caprio, A. Insola, R. Marotta, Catal. Today 53 (1999) 51–59.
[4] N. Oturan, M.H. Zhou, M.A. Oturan, J. Phys. Chem. A 114 (2010) 10605–10611.
[5] H. Roth, Y. Gendel, P. Buzatu, O. David, M. Wessling, J. Hazard. Mater. 307 (2016) 1–6.
[6] W. Liu, Z. Ai, L. Zhang, J. Hazard. Mater. 243 (2012) 257–264.
[7] F.K. Yu, M.H. Zhou, X.M. Yu, Electrochim. Acta 163 (2015) 182–189.
[8] N. Barhoumi, H. Olvera-Vargas, N. Oturan, D. Huguenot, A. Gadri, S. Ammar, E. Brillas, M.A. Oturan, Appl. Catal. B: Environ. 209 (2017) 637–647.
[9] M. Murati, N. Oturan, J.J. Aaron, A. Dirany, B. Tassin, Z. Zdravkovski, M.A. Oturan, Environ. Sci. Pollut. Res. 19 (2012) 1563–1573.
[10] X.H. Li, X.D. Jin, N.N. Zhao, I. Angelidaki, Y.F. Zhang, Bioresour. Technol. Rep. 228 (2017) 322–329.
[11] Y.X. Gong, J.Y. Li, Y.Y. Zhang, M. Zhang, X.J. Tian, A. Wang, J. Hazard. Mater. 304 (2016) 320–328.
[12] G.B. Ren, M.H. Zhou, M.M. Liu, L. Ma, H.J. Yang, Chem. Eng. J. 298 (2016) 55–67.
[13] M. Cheng, G.M. Zeng, D.L. Huang, C. Lai, P. Xu, C. Zhang, Y. Liu, Chem. Eng. J. 284 (2016) 582–598.
[14] T.H. Cheng, C.P. Huang, Y.H. Huang, Y.J. Shih, Chem. Eng. J. 308 (2017) 954–962.
[15] C. Trellu, E. Mousset, Y. Pechaud, D. Huguenot, E.D. van Hullebusch, G. Esposito, M.A. Oturan, J. Hazard. Mater. 306 (2016) 149–174.
[16] H. Dong, H.M. Su, Z. Chen, H. Yu, H.B. Yu, Electrochim. Acta 222 (2016) 1501–1509.
[17] A.D. Bokare, W.Y. Choi, J. Hazard. Mater. 275 (2014) 121–135.
[18] I. Sires, E. Brillas, M.A. Oturan, M.A. Rodrigo, M. Panizza, Environ. Sci. Pollut.Res. 21 (2014) 8336–8367.
[19] C.C. Chen, M. Mo, W.S. Chen, M.Z. Pan, Z.Y. Xu, D.G. Li, Compos. Sci. Technol. 156 (2018) 103–108.
[20] C.M. Dominguez, A. Quintanilla, P. Ocon, J.A. Casas, J.J. Rodriguez, Carbon 60 (2013) 76–83.
[21] H.T. Gomes, S.M. Miranda, M.J. Sampaio, A.M.T. Silva, J.L. Faria, Catal. Today 151 (2010) 153–158.
[22] A. Viinikanoja, Z.J. Wang, J. Kauppila, C. Kvarnstrom, Phys. Chem. Chem. Phys. 14 (2012) 14003–14009.
[23] S. Toh, K. Loh, S. Kamarudin, W. Daud, Chem. Eng. J. 251 (2014) 422–434.
[24] X. Huang, Z. Zeng, Z. Fan, J. Liu, H. Zhang, Adv. Mater. 24 (2012) 5979–6004.
[25] S. Yuan, J.L. Bao, L. Wang, Y. Xia, D.G. Truhlar, Y. Wang, Adv. Energy Mater. 6 (2016) 1501733.
[26] C.C. Chen, D.G. Li, H. Yano, K. Abe, J. Agr. Food. Chem. 67 (2019) 5571–5578.
[27] L.B. Xing, S.F. Hou, J. Zhou, J.L. Zhang, W.J. Si, Y.H. Dong, S.P. Zhuo, J. Solid State Chem. 230 (2015) 224–232.
[28] Y. Wu, F. Yang, X.X. Liu, G.Q. Tan, D. Xiao, Appl. Surf. Sci. 435 (2018) 281–289.
[29] X. Zhu, J. Ni, X. Xing, X. Li, Y. Jiang, Electrochim. Acta 56 (2011) 1270–1274.
[30] L.B. Xing, S.F. Hou, J.L. Zhang, J. Zhou, Z. Li, W. Si, S. Zhuo, Mater. Lett. 147 (2015) 97–100.
[31] W.J. Hou, Y.M. Zhang, T. Liu, H.W. Lu, L. He, RSC Adv. 5 (2015) 8037–8043.
[32] L. Yang, S. Jiang, Y. Zhao, L. Zhu, S. Chen, X. Wang, Q. Wu, J. Ma, Y. Ma, Z. Hu, Angew. Chemie Int. Ed. English 50 (2011) 7132–7135.
[33] Y. Xie, Z. Meng, T.W. Cai, W.Q. Han, ACS Appl. Mater. Inter. 45 (2015) 25202–25210.
[34] S. Longo, M. Mauro, C. Daniel, P. Musto, G. Guerra, Carbon 77 (2014) 896–905.
[35] H. Yu, Y. Li, M. Zhao, H. Dong, H.B. Yu, S.H. Zhan, L. Zhang, Catal. Today 258 (2015) 156–161.
[36] Z.W. Miao, X.G. Gu, S.G. Lu, M.L. Brusseau, N. Yan, Z.F. Qiu, Q. Sui, J. Hazard. Mater. 300 (2015) 530–537.
[37] Y. Xu, K. Sheng, C. Li, G. Shi, ACS Nano 4 (2010) 4324–4330.
[38] S. Chowdhury, Y. Jiang, S. Muthukaruppan, R. Balasubramanian, Carbon 128 (2018) 237–248.
[39] L. Zhang, Z.Y. Zhang, R.P. Liang, Y.-H. Li, J.D. Qiu, Anal. Chem. 86 (2014) 4423–4430.
[40] X. Zhu, J. Ni, X. Xing, X. Li, Y. Jiang, Electrochim. Acta 56 (2011) 1270–1274.
[41] X. Zhang, Z. Sui, B. Xu, S. Yue, Y. Luo, W. Zhan, B. Liu, J. Mater. Chem. 21 (2011) 6494–6497.
[42] Y. Zhang, F. Wang, P. Ou, H. Zhu, Y. Lai, Y. Zhao, J. Hazard. Mater. 360 (2018) 223–232.
[43] X.X. Peng, Y. Tian, S.W. Liu, Chem. Eng. J. 309 (2017) 717–724.
[44] W. Chen, L. Xu, Y. Tian, H. Li, K. Wang, Carbon 137 (2018) 458–466.
[45] T. Liu, K. Wang, S. Song, A. Brouzgou, P. Tsiakaras, Y. Wang, Electrochim. Acta 194 (2016) 228–238.
[46] Y. Zhang, D. Zhang, L. Zhou, Y. Zhao, J. Chen, Z. Chen, F. Wang, J. Chem. Eng. 336 (2017) 690–700.
[47] Z. Chen, Y.M. Zhang, L.C. Zhou, H. Zhu, F. Wang, Y. Wang, D.D. Zhang, J. Hazard. Mater. 332 (2017) 70–78.
[48] W.J. Chen, C.J. Zou, Y. Liu, J. Ind. Eng. Chem. 56 (2017) 428–434.
[49] X. Cao, Z. Yin, H. Zhang, Energy Environ. Sci. 7 (2014) 1850–1865.
[50] P. Ashok, S. Ramaprabhu, J. Colloid. Interf. Sci. 479 (2016) 260–270.
[51] L. Ferrighi, M. Datteo, C. Di Valentin, J. Phys. Chem. C. 118 (2014) 223–230.
[52] G. Fazio, L. Ferrighi, C. Di Valentin, J. Catal. 318 (2014) 203–210.
[53] M.H. Zhou, Q. Yu, L. Lei, G. Barton, Sep. Purif. Technol. 57 (2007) 380.
[54] M. Hartmann, S. Kullmann, H. Keller, J. Mater. Chem. 20 (2010) 9002.
[55] J. Zhang, B. Sun, X.H. Guan, Sep. Purif. Technol. 107 (2013) 48–53.
[56] Y.Y. Zhu, M. Yue, V. Natarajan, RSC Adv. 8 (2018) 14879–14887.
[57] J. Sharma, I.M. Mishra, V. Kumar, J. Environ. Manage. 166 (2016) 12–22.
[58] S. Yuan, N. Gou, A.N. Alshawabkeh, A.Z. Gu, Chemosphere. 93 (2013) 2796–2804.
[59] W. Wu, Z.H. Huang, T.T. Lim, J. Environ.Chem. Eng. 4 (2016) 2807–2815.